Nano Research
DOI 10.1007/s12274-013-0346-2
Research Article

ISSN 1998-0124
CN 11-5974/O4

Thickness-dependent patterning of MoS_2 sheets with well-oriented triangular pits by heating in air

Haiqing Zhou[1,2], Fang Yu[5], Yuanyue Liu[3,4], Xiaolong Zou[3,4], Chunxiao Cong[1], Caiyu Qiu[1], Ting Yu[1] (✉), Zheng Yan[2], Xiaonan Shen[1], Lianfeng Sun[5], Boris I. Yakobson[2,3,4] (✉), and James M. Tour[2,3,4] (✉)

[1] *Division of Physics and Applied Physics, School of Physical and Mathematical Sciences, Nanyang Technological University, 637371, Singapore*
[2] *Department of Chemistry, Rice University, 6100 Main Street, Houston, Texas 77005, USA*
[3] *The Smalley Institute for Nanoscale Science and Technology, Rice University, 6100 Main Street, Houston, Texas 77005, USA*
[4] *Department of Mechanical Engineering and Materials Science, Rice University, 6100 Main Street, Houston, Texas 77005, USA*
[5] *National Center for Nanoscience and Technology, Beijing 100190, China*

Received: 31 May 2013
Revised: 27 June 2013
Accepted: 30 June 2013

© Tsinghua University Press and Springer-Verlag Berlin Heidelberg 2013

KEYWORDS
layered MoS_2, oxidative etching, thickness-dependent, triangular pits

ABSTRACT

Patterning ultrathin MoS_2 layers with regular edges or controllable shapes is appealing since the properties of MoS_2 sheets are sensitive to the edge structures. In this work, we have introduced a simple, effective and well-controlled technique to etch layered MoS_2 sheets with well-oriented equilateral triangular pits by simply heating the samples in air. The anisotropic oxidative etching is greatly affected by the surrounding temperature and the number of MoS_2 layers, whereby the pit sizes increase with the increase of surrounding temperature and the number of MoS_2 layers. First-principles computations have been performed to explain the formation mechanism of the triangular pits. This technique offers an alternative avenue to engineering the structure of MoS_2 sheets.

1 Introduction

As a layered semiconducting analogue of graphene, molybdenum disulfide (MoS_2) has attracted considerable attention due to the intriguing existence of a bandgap in its electronic structure, which is complementary to graphene-based electronic behaviors [1–5]. Similar to noble metal nanoparticles [6] and metal thin films [7–9], as the thickness of MoS_2 sheets decreases from the bulk MoS_2 crystal to monolayer (1L) MoS_2, new layer-dependent chemical and physical properties arise in ultrathin MoS_2 layers, such as the indirect-to-direct transitions [1, 10], photoluminescence emergence [11], and alterations in Raman signals [12–14]. These can be ascribed to the quantum confinement effects which become significant as MoS_2 is scaled down from three- to two-dimensional geometry. Since layered MoS_2 sheets are typical

Address correspondence to James M. Tour, tour@rice.edu; Ting Yu, yuting@ntu.edu.sg; Boris I. Yakobsen, biy@rice.edu

TSINGHUA UNIVERSITY PRESS Springer

semiconductors [1], we conjecture that the surface chemical reactivities of MoS_2 sheets are dependent on their thickness as observed in metal thin films [9] or graphene [15]. Interestingly, according to theoretical and experimental studies, the electrical, magnetic, and electrochemical properties of thin MoS_2 layers, especially quantum-confined nanostructures, are greatly affected by their edge structures [16, 17]. For example, it has been long-realized that MoS_2 can serve as a hydrodesulphurization (HDS) or hydrogen evolution reduction (HER) catalyst, in which the number of exposed active edge sites plays an important role during the catalytic process [18, 19]. Since the basal planes of MoS_2 sheets are usually catalytically inert, engineering the surface structure of thin MoS_2 layers with an abundance of exposed active edge sites could provide an important route for MoS_2-based electrocatalysis modification.

In this work, using a dry oxygen etching reaction, we report a new avenue to chemically etch ultrathin MoS_2 layers with regular edges or controlled shapes in a crystallographic oriented manner by simply heating the MoS_2 samples in air with controlled temperature. We find that ultrathin MoS_2 layers tend to be etched with equilateral triangular pits. These triangular pits, which potentially expose a great number of catalytically active edge sites, are surprisingly well-oriented, and their sizes are dependent on the surrounding temperature and the number of MoS_2 layers. Based on first-principles calculations, an atomic mechanism is proposed to explain the formation and orientation of triangular pits in MoS_2 layers. Furthermore, using Raman and photoluminescence (PL) spectroscopy, oxygen-induced hole doping can be detected on the basal plane of MoS_2 sheets.

2 Experimental

Similar to graphene preparation [20–22], pristine n-layer MoS_2 was mechanically exfoliated from commercially available bulk MoS_2 crystals (SPI Supplies), and then transferred onto the SiO_2/Si substrates. Optical microscopy (Leica DM 4000) and micro-Raman spectroscopy (Renishaw inVia Raman microscope) were used to determine the thickness of ultrathin MoS_2 sheets (Fig. S1 (in the Electronic Supplementary Material (ESM))).

The mechanically exfoliated MoS_2 samples were placed in a quartz tube, in the centre of a tubular furnace at temperatures above 250 °C and below 385 °C with precise modulation. The heating process was carried out with a rate of ~20 to 25 °C/min. During thermal heating for about 2 h, no carrier or reactive gas was introduced into the tubular furnace, and the two ends of the quartz tube were uncovered. After the etching process, the samples were allowed to cool to room temperature under ambient conditions.

The micro-Raman spectroscopy (Renishaw inVia Raman microscope) experiments were carried out under ambient conditions with 514.5 nm laser excitation. In order to avoid laser induced heating of samples, the laser power was set below 1.0 mW. The application of a 100 × objective lens with a numerical aperture of 0.90 can provide a ~1 μm laser spot size, and the spatial resolution is below 1 μm. Many Raman spectra were collected to ensure the credibility and repeatability of the results. PL measurements were performed by a WITEC CRM200 system using an excitation energy of 532 nm (2.33 eV). The PL spectra were collected at ~200 μW laser power for 20 s.

3 Results and discussion

The ultrathin MoS_2 sheets were placed on SiO_2/Si substrates as shown (Fig. 1(a)). This fabrication procedure is very similar to the technique for graphene preparation [20–22]. Optical microscopy and Raman spectroscopy were used to identify the number of

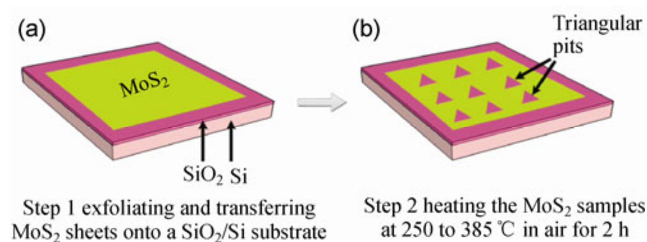

Figure 1 A schematic diagram showing the technique of oxidative etching in the experiment. (a) Mechanically exfoliating and transferring n-layer MoS_2 sheets onto a silicon substrate with a 300 nm SiO_2 layer. (b) Heating the MoS_2 samples in air at various temperatures.

MoS_2 layers on the basis of color contrast and peak frequency difference (Fig. S1 (in the ESM)) [12–14, 23, 24]. Subsequently, the MoS_2 samples were placed in a tube furnace for heating in air for 2 h with controlled temperature from 250 °C to 385 °C and atmospheric pressure (Fig. 1(b)). The samples were further characterized by atomic force microscopy (AFM), Raman and PL spectroscopy to study the anisotropic etching.

Graphene can be tailored with hexagonal pits or regular trenches with angles of 60° or 120° between two adjacent trenches by anisotropic etching, which includes oxygen [25, 26] and hydrogen plasma etching [27, 28], or by catalytic hydrogenation of carbon [29, 30]. Even though ultrathin MoS_2 layers show hexagonal layered-lattice crystal structures similar to graphene or layered hexagonal BN (h-BN), 1L MoS_2 is clearly different in that it is composed of three atomic layers: A Mo layer sandwiched between two S layers. The bonding in each S–Mo–S trilayer is mainly covalent in nature, and is thus strong, while the S–Mo–S trilayers are held together through van der Waals interactions. In the light of this difference, when ultrathin MoS_2 sheets are exposed to anisotropic oxidative etching [31], some differences between this material and graphene are observed.

By directly heating the MoS_2 samples in air at various temperatures, we have surprisingly found that 1L MoS_2 tends to be etched with a series of triangular pits (Fig. 2), in which most of the angles are close to 60°(Fig. S2 (in the ESM)). Also, all the triangular pits are oriented in the same direction and have a uniform size distribution (Fig. S3 (in the ESM)). As shown in Figs. 2(b)–2(d), it is seen that, in a typical equilateral triangle, one side is always parallel to the white-marked long dashed lines, and the other two sides lie at an angle of 60° or 120° with these long dashed lines. These triangular structures are consistent with recently published results on the growth of single crystal MoS_2 grains by the chemical vapor deposition (CVD) method [32–34], in which the single grains exhibit a triangular shape. Considering the special lattice structures of layered MoS_2, the triangular shape of the etched pits may imply that their edges are parallel to a specific crystallographic direction [16, 18, 35], and only one edge termination is energetically favored. Moreover, with the increase of surrounding temperature, the etching process increases. Namely, when the surrounding temperature is below 325 °C, almost no etching effect can be detected by AFM (Fig. S4 (in the ESM)). In sharp contrast, at 345 °C, 355 °C or 365 °C, obvious triangular pits can be found in the AFM images, and the triangle side becomes longer as the temperature increases (Figs. S3 and S5 (in the ESM)), and seems to exhibit a linear relationship with the surrounding temperature (Fig. S6 (in the ESM)). The triangles remain well-oriented in the same direction with the increase in etching temperature, but the distortions might result from the harsh, fast oxidative etching rate with increasing temperature.

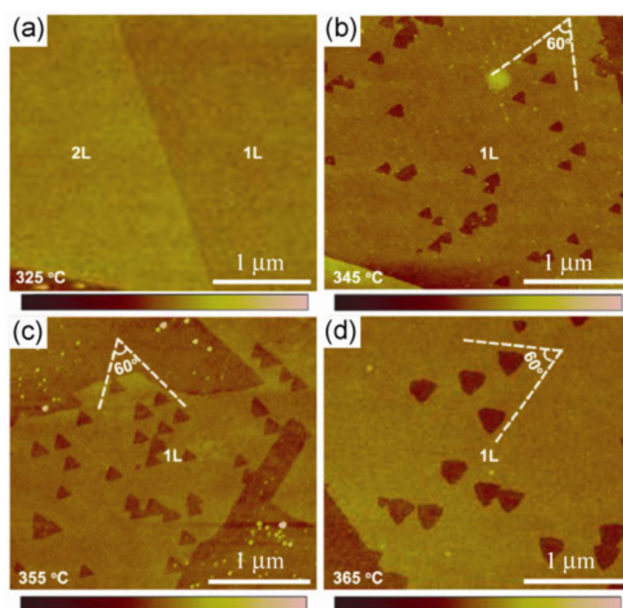

Figure 2 Typical AFM images showing the formation of well-oriented equilateral triangular pits on 1L MoS_2 at various temperatures: (a) 325 °C, (b) 345 °C, (c) 355 °C, and (d) 365 °C. It is interesting to note that these triangular pits are formed with a common orientation, and their sizes increase with the increase of annealing temperature.

Because no highly oxidative and poisonous XeF_2 gas [36], high-power laser irradiation [37] or lithography patterning [38] are involved during the heating process, the technique reported here is less expensive, simpler, safer and time-saving when compared to the reported etching methods for MoS_2 flakes [36–38]. The well-oriented triangular pits are easily fabricated on layered MoS_2 sheets by means of oxidative etching.

Even so, this technique can only be used to pattern MoS_2 with triangular pits, rather than shapes such as hexagonal pits or nanoribbons. This is because oxidative etching is greatly affected by the edge orientations of layered MoS_2 sheets. Since gas-phase O_2 directly reacts with the MoS_2 surface without the need for any masks such as graphene [36], the formation of equilateral triangular pits with good orientation is unique to layered MoS_2 sheets and dominated by the special lattice structure of MoS_2 as suggested by our theoretical calculations.

Interestingly, the anisotropic oxidative etching is dependent on the number of MoS_2 layers. As shown in Fig. 3, the sizes or side lengths of the triangular pits on n-layer MoS_2 are obviously different among ultrathin MoS_2 layers of different thicknesses. For example, after oxidative etching at 355 °C (Figs. 3(a) and 3(c)), the average pit sizes are the smallest on 1L MoS_2, while for other MoS_2 layers, the relevant triangular pit sizes progressively increase from bilayer (2L) to quadrilayer (4L). Similarly, as shown in Figs. 3(b) and 3(d), when the temperature is 365 °C, the average pit sizes on multilayer (ML $\geqslant$ 10 layers) MoS_2 are much larger than that on 1L MoS_2. These results suggest the thickness-dependent behavior of oxidative etching on MoS_2 sheets, which is further confirmed by the complete etching of few layer MoS_2 and 1L MoS_2 remaining unetched at 375 °C (Fig. S7 (in the ESM)) [38], and the observation of lots of triangular pits on thick MoS_2 (Fig. S9 (in the ESM)). Note that it is somewhat difficult to find triangular pits on thick MoS_2 layers by AFM height profiles (Figs. 3(a) and 3(b)), but it is easier to detect them from the corresponding AFM phase images (Figs. 3(c) and 3(d)), indicating AFM phase imaging can provide complementary information to the topography image. The difficulty in clearly detecting the triangular pits in the AFM topology images may be due to the height difference between the etched and non-etched regions for multilayer MoS_2 stacked with thin MoS_2, since only the uppermost as well as the underlying second layer are likely etched at these temperatures. It is possible to find the triangular pits on an individual thick MoS_2 flake (Fig. S9 (in the ESM)). Nonetheless, from the AFM phase images, each triangle is composed of three equilateral sides for almost all the MoS_2 layers.

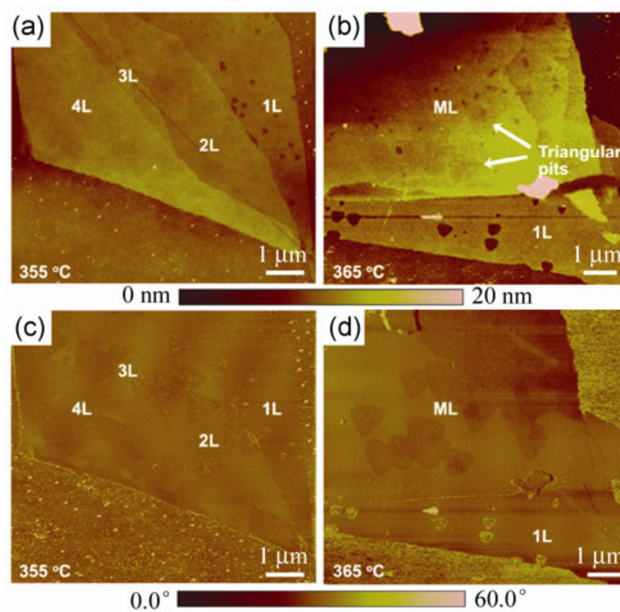

Figure 3 Typical AFM height profiles (a) and (b), and corresponding phase images (c) and (d) showing the thickness-dependent oxidative etching of MoS_2 sheets with well-oriented triangular pits. (a) and (c) 355 °C. (b) and (d) 365 °C. The average size of the triangular pits on 1L MoS_2 is smaller than that for thicker multilayer (ML) MoS_2 sheets.

The triangular shape of the etched pits originates from the anisotropic oxidation of MoS_2 edges, as shown in Fig. 4. The pit expands through chemical oxidation of its edges, where the Mo and S atoms become MoO_3 and SO_2 gas molecules, respectively [39, 40]. Different edge directions could have different reaction rates, resulting in different rates of anisotropic etching along these directions. Eventually, the pit will converge to a regular shape determined by the kinetic Wulff construction [41, 42]: The fast-etching edges disappear fast, leaving the pit essentially composed of the slow-etching edges. Although MoS_2 has various edges, their structures and energies can be represented by three main types: Mo-terminated zigzag (ZZ-Mo), S_2-terminated zigzag (ZZ-S_2) and armchair (AC) edges similar to graphene [42–44]. The pit cannot be composed of AC edges, since it would have a hexagonal shape due to the six-fold symmetry of AC directions. Thus, the etched pit is likely to have ZZ edges, either ZZ-Mo or ZZ-S_2. The alignment of the edges between the pits and the MoS_2 layer also implies that the pit edges should be ZZ since the MoS_2 layer typically exposes ZZ edges [16, 18, 35]. To further demonstrate the different etching rates between ZZ-Mo and ZZ-S_2,

we identify the most exothermic reaction path for each edge by performing first-principles computations. The detailed description of calculations can be found in the ESM. The atomic structures and energy evolution during chemical oxidation are shown in Fig. 4, where the energy ΔE is defined as the enthalpy change (normalized by the edge length) from one edge structure to another, by incorporating O_2 and evaporating MoO_3 or SO_2 gas molecules. Starting from the ZZ-Mo edge (bottom panel), the oxygen reacts first with Mo and then S, while for ZZ-S_2, the reaction is in the reverse order. Notably, significant structural reconstructions are found in both cases. During the etching of ZZ-Mo, the energy drops monotonically, while for ZZ-S_2, there is a plateau, suggesting that the ZZ-S_2 edge probably propagates more slowly than in the ZZ-Mo edge, and thus appears at the etched pit. Even though a detailed examination of an atom-by-atom reaction path is beyond the scope of this work, Fig. 4 is already informative to explain why the etched pits are all triangular with the same crystallographic orientation. This explanation is further supported by the observations of the inverse triangles in MoS_2 layers (Fig. S10 (in the ESM)). If the MoS_2 sheets follow the lowest-energy stacking AA′ order as that in bulk MoS_2 (the Mo atoms in the next layer are directly on top of the S atom in the first layer and vice versa), the ZZ-Mo and ZZ-S_2 directions should be reversed in the two neighboring layers, leading to the opposite orientation of the pits upon oxidative etching, which seems to agree with our experimental results as shown in Fig. S10 (in the ESM).

In order to rationalize out the thickness-dependent etching behaviors, it is necessary for us to consider the thermodynamic (e.g., energetics and stability) and kinetic (e.g., surface diffusion) factors. According to our experimental results (Figs. 2, 3, and S3 (in the ESM)), the etched pits are uniform in size and shape for the MoS_2 samples. This means that the oxidative etching is likely to be initiated at preexisting structural defects [45–47], rather than on vacancies formed during the oxidation on the surface of MoS_2 samples,

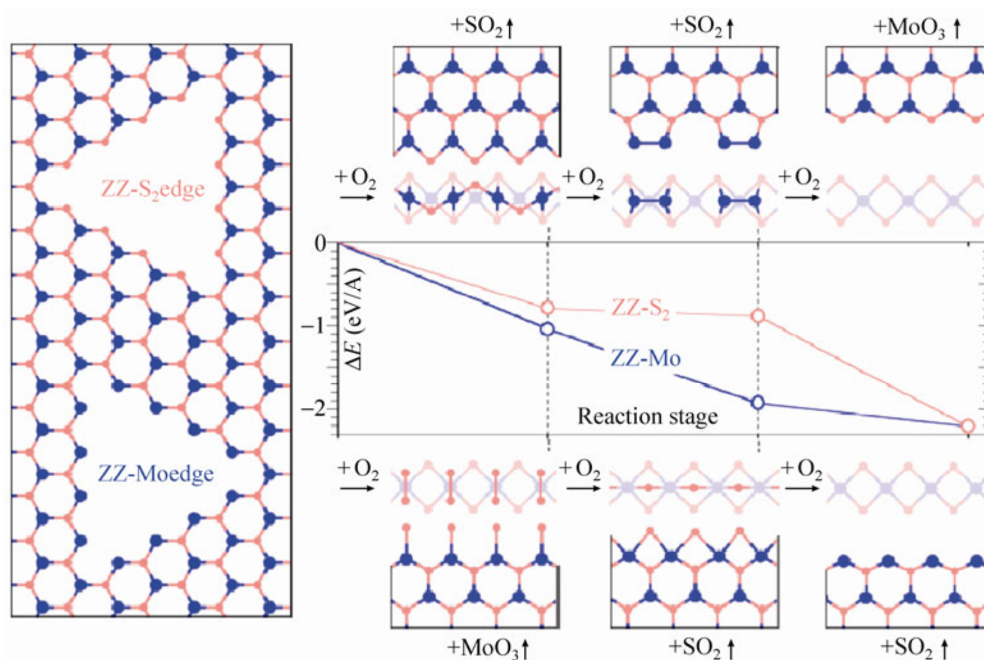

Figure 4 An atomic mechanism showing the formation of triangular pits in MoS_2 layers. A pit in MoS_2 could generally expose various types of edges, including ZZ-Mo and ZZ-S_2, as shown on the left. The Mo and S atoms are represented by large (blue) and small (red) circles, respectively. Right: The atomic edge structures (top and side views) during oxidation of ZZ-Mo are shown in the bottom panels, and those for ZZ-S_2 are displayed in the top panels. In the side views, only two ZZ rows near the edge are rendered for clarity, where the deeper one is shown in pale color. The edge energy variations during oxidation are shown in the middle, where the energy of the oxygen-intact edge is set as zero.

which occurs only at higher temperatures. Also, for lower oxygen partial pressure (5% oxygen in argon), the etched pits are still uniform in size and shape (Fig. S11 (in the ESM)), which further supports the conclusion that the triangular pits are initiated probably at natural surface defects of MoS_2. The pit density is a little lower, which is attributed to the possible change of activation energy barriers at the initial etching stage, or surface diffusion coefficients of oxygen on MoS_2 basal plane under different oxygen partial pressures [45]. Meanwhile, the triangular pit sizes are dependent on the number of MoS_2 layers, with 1L MoS_2 having the smallest pit sizes, which indicates the lowest etching rate is found on a 1L MoS_2 surface [38]. Thus, this thickness-dependent etching or patterning of ultrathin MoS_2 layers can be mainly attributed to size-dependent surface chemical reactivity, which may originate from the weak van der Waals coupling between MoS_2 layers and possibly different oxygen coverage adsorbed on n-layer MoS_2 sheets [9, 22]. In view of the similar oxidative etching on graphene [21], it may be possible to fabricate 1L MoS_2 from few-layer or thick MoS_2 (Fig. S8 (in the ESM)) by further optimizing the oxygen gas concentration, etching temperature, chamber pressure and flow rates. Similar to graphite, there are two possible independent reaction mechanisms for the growth of etch pits in these experiments [45–47]: One is the reaction initiated by direct interactions of gas-phase O_2 with reactive defective sites on the MoS_2 surface (Eley–Rideal (ER) mechanism). The second is the surface migration mechanism: Reaction of MoS_2 with the migrating O_2 molecules that are first chemisorbed and then diffuse to encounter the active sites on the MoS_2 basal plane (Langmuir–Hinshelwood mechanism). In this sense, it is reasonable for us to conclude that the MoS_2 samples with different thicknesses could have different oxidative etching rates. The thickness of MoS_2 flakes might play a role in the adsorption, diffusivity, and reactivity of O_2 on MoS_2. The detailed mechanism needs further experimental and theoretical investigations.

Raman and PL spectroscopy have been used to further characterize oxygen-etched ultrathin MoS_2 layers; the spectra are shown in Figs. 5 and S12 (in the ESM). For comparison, the Raman and PL spectra of pristine 1L and 2L MoS_2 are also displayed. From these Raman spectra, we can conclude that some red shifts of the E^1_{2g} mode and blue shifts of the A_{1g} mode are present for 1L and 2L MoS_2 after oxidative etching (Fig. S13 (in the ESM)). Also, the frequency differences ($\omega_{A_{1g}} - \omega_{E^1_{2g}}$) and intensity ratios between E^1_{2g} and A_{1g} modes have changed (Fig. 5). That is, the frequency differences vary from 18.0 cm^{-1} to 19.4 cm^{-1} for 1L MoS_2, and 21.3 cm^{-1} to 22.5 cm^{-1} for 2L MoS_2. The intensity ratios between A_{1g} and E^1_{2g} modes increase from 1.28 to 1.46 for 1L MoS_2, and 0.69 to 1.0 for 2L MoS_2. Additionally, compared to the pristine states, the PL spectra of etched 1L and 2L MoS_2 have undergone some changes: The peak shape becomes much sharper, and the corresponding PL intensity is enhanced greatly, which are probably due to the decrease of electron density resulting from oxygen-induced hole doping and sulfur-rich defect states after oxidative etching [48]. These prominent Raman and PL features may originate from the oxygen-induced hole doping [49, 50], rather than lattice deformation induced by thermal annealing. Additionally, after oxidative etching, the Raman peaks are very similar to those of the pristine MoS_2 samples (Fig. S12), with no Raman signals due to the presence of MoO_3 detected under the experimental conditions, indicating no solid-state MoO_3 was synthesized.

4 Conclusions

We have reported the thickness-dependent oxidative etching of ultrathin MoS_2 layers with the generation of well-oriented triangular pits by simply heating MoS_2 samples in air under various temperatures, which can be explained by theoretical calculations. This oxidative etching can help us to change the ratio of basal plane sites to edge sites, which can be used as an alternative technique to introduce a great number of catalytically active edge sites into the inert basal plane of MoS_2. These MoS_2 triangles could potentially enable new opportunities to enhance surface properties for MoS_2-based HDS or HER catalysis [18, 19], and to engineer electronic structures of ultrathin MoS_2 layers.

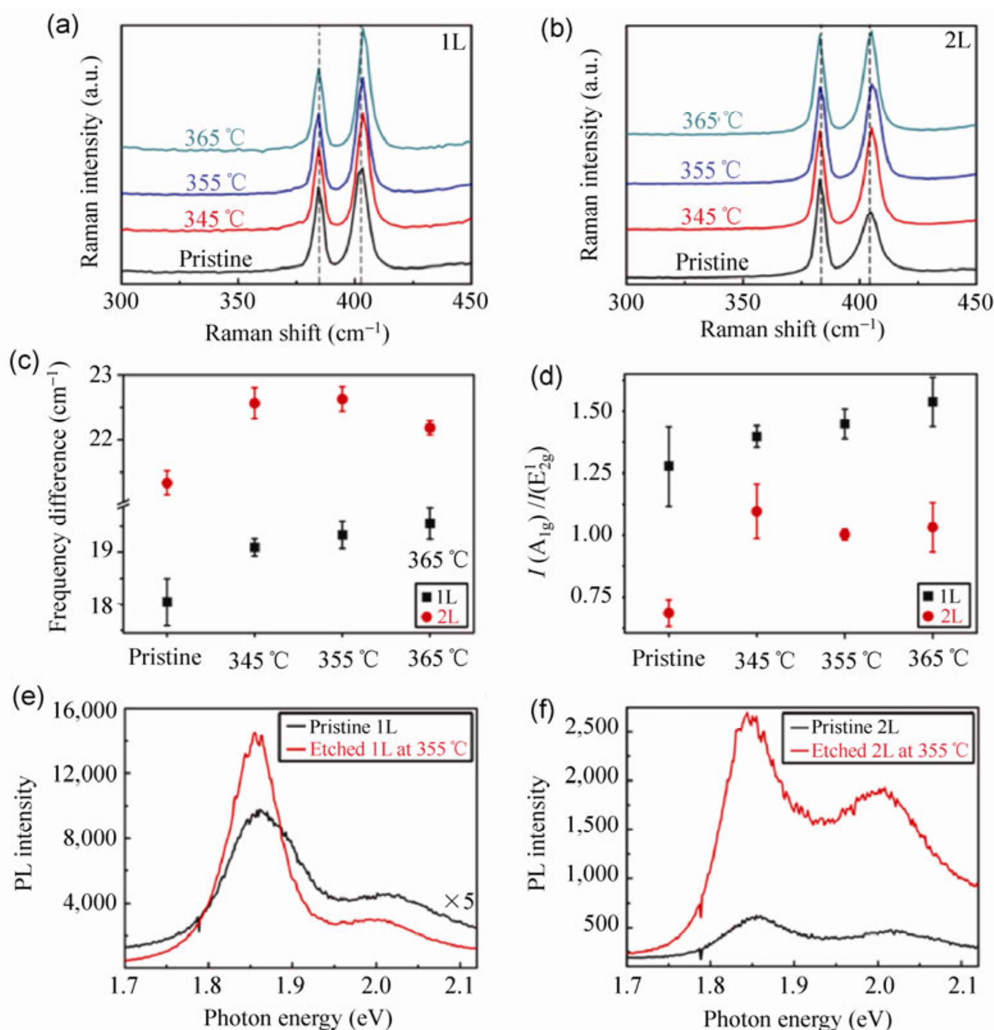

Figure 5 The micro-Raman spectra, corresponding Raman parameters (the frequency difference and intensity ratio) and PL spectra of pristine and oxidized MoS_2 sheets under various temperatures. (a) and (b) Comparison of the Raman spectra of (a) 1L and (b) 2L MoS_2 simply heated in air at different temperatures. (c) and (d) The frequency differences ($\omega_{A_{1g}} - \omega_{E^1_{2g}}$) and intensity ratios between E^1_{2g} and A_{1g} for 1L (black) and 2L (red) MoS_2 simply heated in air at different temperatures. (e) PL spectra of pristine and oxygen-etched 1L MoS_2 at 355 ℃. (f) PL spectra of pristine and oxygen-etched 2L MoS_2 at 355 ℃. All the Raman spectra were recorded at room temperature by 514.5 nm laser excitation with a laser power of ~0.5 mW and laser spot size of ~1 μm.

Acknowledgements

This project was supported by the Singapore National Research Foundation (NRF) under NRF Research Foundation (RF) Award No. NRF-RF2010-07, National Science Foundation of China (Grant Nos. 10774032 and 90921001), the Air Force Office of Scientific Research (AFOSR) Multidisciplinary University Research Initiative (MURI) (No. FA9550-12-1-0035), the U. S. Army Research MURI (No. W911NF-11-1-0362) and the AFOSR (No. FA9550-09-1-0581).

Electronic Supplementary Material: Computational methods, thickness determination of n-layer MoS_2, statistical analysis of the angles and size of triangular pits, height measurements on 1L MoS_2 before and after oxidative etching, oxidative etching rate varying with temperature, optical images of n-layer MoS_2 before and after oxidative etching at 375 ℃ or 385 ℃, AFM characterization of oxygen-etched thick MoS_2, experimental observation of the inverse triangles in MoS_2 layers, AFM images of etched MoS_2 sheets with 5% oxygen in argon, and Raman spectra of n-layer

MoS_2 sheets after oxidative etching. This material is available in the online version of this article at http://dx.doi.org/10.1007/s12274-013-0346-2.

References

[1] Mak, K. F.; Lee, C.; Hone, J.; Shan, J.; Heinz, T. F. Atomically thin MoS_2: A new direct-gap semiconductor. *Phys. Rev. Lett.* **2010**, *105*, 136805.

[2] Radisavljevic, B.; Radenovic, A.; Brivio, J.; Giacometti, V.; Kis, A. Single-layer MoS_2 transistors. *Nat. Nanotechnol.* **2011**, *6*, 147–150.

[3] Wang, Q. H.; Kalantar-Zadeh, K.; Kis, A.; Coleman, J. N.; Strano, M. S. Electronics and optoelectronics of two-dimensional transition metal dichalcogenides. *Nat. Nanotechnol.* **2012**, *7*, 699–712.

[4] Geim, A. K.; Novoselov, K. S. The rise of graphene. *Nat. Mater.* **2007**, *6*, 183–191.

[5] Neto, A. H. C.; Guinea, F.; Peres, N. M. R.; Novoselov, K. S.; Geim, A. K. The electronic properties of graphene. *Rev. Mod. Phys.* **2009**, *81*, 109–162.

[6] Valden, M.; Lai, X.; Goodman, D. W. Onset of catalytic activity of gold clusters on titania with the appearance of nonmetallic properties. *Science* **1998**, *281*, 1647–1650.

[7] Guo, Y.; Zhang, Y. F.; Bao, X. Y.; Han, T. Z.; Tang, Z.; Zhang, L. X.; Zhu, W. G.; Wang, E. G.; Niu, Q.; Qiu, Z. Q. et al. Superconductivity modulated by quantum size effects. *Science* **2004**, *306*, 1915–1917.

[8] Ma, L.Y.; Tang, L.; Guan, Z. L.; He, K.; An, K.; Ma, X. C.; Jia, J. F.; Xue, Q. K. Quantum size effect on adatom surface diffusion. *Phys. Rev. Lett.* **2006**, *97*, 266102.

[9] Ma, X. C.; Jiang, P.; Qi, Y.; Jia, J. F.; Yang, Y.; Duan, W. H.; Li, W. X.; Bao, X. H.; Zhang, S. B.; Xue, Q. K. Experimental observation of quantum oscillation of surface chemical reactivities. *Proc. Natl Acad. Sci. U.S.A.* **2007**, *104*, 9204–9208.

[10] Ellis, J. K.; Lucero, M. J.; Scuseria, G. E. The indirect to direct band gap transition in multilayered MoS_2 as predicted by screened hybrid density functional theory. *Appl. Phys. Lett.* **2011**, *99*, 261908.

[11] Splendiani, A.; Sun, L.; Zhang, Y. B.; Li, T. S.; Kim, J.; Chim, C. Y.; Galli, G.; Wang, F. Emerging photoluminescence in monolayer MoS_2. *Nano Lett.* **2010**, *10*, 1271–1275.

[12] Lee, C. G.; Yan, H. G.; Brus, L. E.; Heinz, T. F.; Hone, J.; Ryu, S. Anomalous lattice vibrations of single- and few-layer MoS_2. *ACS Nano* **2010**, *4*, 2695–2700.

[13] Wang, Y. L.; Cong, C. X.; Qiu, C. Y.; Yu, T. Raman spectroscopy study of lattice vibration and crystallographic orientation of monolayer MoS_2 under uniaxial strain. *Small*, in press, DOI: 10.1002/smll.201202876.

[14] Zhan, Y. J.; Liu, Z.; Najmaei, S.; Ajayan, P. M.; Lou, J. Large-area vapor-phase growth and characterization of MoS_2 atomic layers on a SiO_2 substrate. *Small* **2012**, *8*, 966–971.

[15] Liu, L.; Ryu, S.; Tomasik, M. R.; Stolyarova, E.; Jung, N.; Hybertsen, M. S.; Steigerwald, M. L.; Brus, L. E.; Flynn, G. W. Graphene oxidation: Thickness-dependent etching and strong chemical doping. *Nano Lett.* **2008**, *8*, 1965–1970.

[16] Helveg, S.; Lauritsen, J. V.; Lægsgaard, E.; Stensgaard, I.; Nørskov, J. K.; Clausen, B. S. Atomic-scale structure of single-layer MoS_2 nanoclusters. *Phys. Rev. Lett.* **2000**, *84*, 951–954.

[17] Li, Y. F.; Zhou, Z.; Zhang, S. B.; Chen, Z. F. MoS_2 nanoribbons: High stability and unusual electronic and magnetic properties. *J. Am. Chem. Soc.* **2008**, *130*, 16739–16744.

[18] Jaramillo, T. F.; Jørgensen, K. P.; Bonde, J.; Nielsen, J. H.; Horch, S.; Chorkendorff, I. Identification of active edge sites for electrochemical H_2 evolution from MoS_2 nanocatalysts. *Science* **2007**, *317*, 100–102.

[19] Kibsgaard, J.; Chen, Z. B.; Reinecke, B. N.; Jaramillo, T. F. Engineering the surface structure of MoS_2 to preferentially expose active edge sites for electrocatalysis. *Nat. Mater.* **2012**, *11*, 963–969.

[20] Novoselov, K. S.; Jiang, D.; Schedin, F.; Booth, T. J.; Khotkevich, V. V.; Morozov, S. V.; Geim, A. K. Two-dimensional atomic crystals. *Proc. Natl Acad. Sci. U.S.A.* **2005**, *102*, 10451–10453.

[21] Cong, C. X.; Yu, T.; Wang, H. M.; Zheng, K. H.; Gao, P. Q.; Chen, X. D.; Zhang, Q. Self-limited oxidation: A route to form graphene layers from graphite by one-step heating. *Small* **2010**, *6*, 2837–2841.

[22] Zhou, H. Q.; Qiu, C. Y.; Liu, Z.; Yang, H. C.; Hu, L. J.; Liu, J.; Yang, H. F.; Gu, C. Z.; Sun, L. F. Thickness-dependent morphologies of gold on n-layer graphenes. *J. Am. Chem. Soc.* **2010**, *132*, 944–946.

[23] Castellanos-Gomez, A.; Agraït, N.; Rubio-Bollinger, G. Optical identification of atomically thin dichalcogenide crystals. *Appl. Phys. Lett.* **2010**, *96*, 213116.

[24] Benameur, M. M.; Radisavljevic, B.; Héron, J. S.; Sahoo, S.; Berger, H.; Kis, A. Visibility of dichalcogenide nanolayers. *Nanotechnology* **2011**, *22*, 125706.

[25] Nemes-Incze, P.; Magda, G.; Kamarás, K.; Biró, L. P. Crystallographically selective nanopatterning of graphene on SiO_2. *Nano Res.* **2010**, *3*, 110–116.

[26] Ajayan, P. M.; Yakobson, B. I. Materials science: Oxygen breaks into carbon world. *Nature* **2006**, *7095*, 818–819.

[27] Yang, R.; Zhang, L. C.; Wang, Y.; Shi, Z. W.; Shi, D. X.; Gao, H. J.; Wang, E. G.; Zhang, G. Y. An anisotropic etching

effect in the graphene basal plane. *Adv. Mater.* **2010**, *22*, 4014–4019.

[28] Shi, Z. W.; Yang, R.; Zhang, L. C.; Wang, Y.; Liu, D. H.; Shi, D. X.; Wang, E. G.; Zhang, G. Y. Patterning graphene with zigzag edges by self-aligned anisotropic etching. *Adv. Mater.* **2011**, *23*, 3061–3065.

[29] Ci, L. J.; Song, L.; Jariwala, D.; ElÍas, A. L.; Gao, W.; Terrones, M.; Ajayan, P. M. Graphene shape control by multistage cutting and transfer. *Adv. Mater.* **2009**, *21*, 4487–4491.

[30] Gao, L. B.; Ren, W. C.; Liu, B. L.; Wu, Z. S.; Jiang, C. B.; Cheng, H. M. Crystallographic tailoring of graphene by nonmetal SiO_x nanoparticles. *J. Am. Chem. Soc.* **2009**, *131*, 13934–13936.

[31] Kim, Y.; Huang, J. L.; Lieber, C. M. Characterization of nanometer scale wear and oxidation of transition metal dichalcogenide lubricants by atomic force microscopy. *Appl. Phys. Lett.* **1991**, *59*, 3404.

[32] Wu, S. F.; Huang, C. M.; Aivazian, G.; Ross, J. S.; Cobden, D. H.; Xu, X. D. Vapor-solid growth of high optical quality MoS_2 monolayers with near-unity valley polarization. *ACS Nano* **2013**, *7*, 2768–2772.

[33] van der Zande, A. M.; Huang, P. Y.; Chenet, D. A.; Berkelbach, T. C.; You, Y. M.; Lee, G. H.; Heinz, T. F.; Reichman, D. R.; Muller, D. A.; Hone, J. C. Grains and grain boundaries in highly crystalline monolayer molybdenum disulphide. *Nat. Mater.* **2013**, *12*, 554–561.

[34] Najmaei, S.; Liu, Z.; Zhou, W.; Zou, X. L.; Shi, G.; Lei, S. D.; Yakobson, B. I.; Idrobo, J. C.; Ajayan, P. M.; Lou, J. Vapour phase growth and grain boundary structure of molybdenum disulphide atomic layers. *Nat. Mater.* **2013**, in press, DOI: 10.1038/NMAT3673.

[35] Schweiger, H.; Raybaud, P.; Kresse, G.; Toulhoat, H. Shape and edge sites modifications of MoS_2 catalytic nanoparticles induced by working conditions: A theoretical study. *J. Catal.* **2002**, *207*, 76–87.

[36] Huang, Y.; Wu, J.; Xu, X. F.; Ho, Y. D.; Ni, G. X.; Zou, Q.; Koon, G. K. W.; Zhao, W. J.; Shen, C. M.; Castro Neto, A. H. et al. An innovative way of etching MoS_2: Characterization and mechanism investigation. *Nano Res.* **2013**, *6*, 200–207.

[37] Liu, H.; Gu, J. J.; Ye, P. D. MoS_2 nanoribbon transistors: Transition from depletion mode to enhancement mode by channel-width trimming. *IEEE Electr. Device L.* **2012**, *33*, 1273–1275.

[38] Castellanos-Gomez, A.; Barkelid, M.; Goossens, A. M.; Calado, V. E.; van der Zant, H. S. J.; Steele, G. A. Laser-thinning of MoS_2: On demand generation of a single-layer semiconductor. *Nano Lett.* **2012**, *12*, 3187–3192.

[39] Ross, S.; Sussman, A. Surface oxidation of molybdenum disulfide. *J. Phys. Chem.* **1955**, *59*, 889–892.

[40] Lince, J. R.; Frantz, P. P. Anisotropic oxidation of MoS_2 crystallites studied by angle-resolved X-ray photoelectron spectroscopy. *Tribol. Lett.* **2000**, *9*, 211–218.

[41] Sekerka, R. F. Equilibrium and growth shapes of crystals: How do they differ and why should we care? *Cryst. Res. Technol.* **2005**, *40*, 291–306.

[42] Artyukhov, V. I.; Liu, Y.; Yakobson, B. I. Equilibrium at the edge and atomistic mechanisms of graphene growth. *Proc. Natl. Acad. Sci. U.S.A.* **2012**, *109*, 15136–15140.

[43] Liu, Y.; Dobrinsky, A.; Yakobson, B. I. Graphene edge from armchair to zigzag: The origins of nanotube chirality? *Phys. Rev. Lett.* **2010**, *105*, 235502.

[44] Liu, Y.; Bhowmick, S.; Yakobson, B. I. BN white graphene with “colorful” edges: The energies and morphology. *Nano Lett.* **2011**, *11*, 3113–3116.

[45] Yang, R. T.; Wong, C. Kinetics and mechanism of oxidation of basal plane on graphite. *J. Chem. Phys.* **1981**, *75*, 4471–4476.

[46] Chang, H.; Bard, A. J. Formation of monolayer pits of controlled nanometer size on highly oriented pyrolytic graphite by gasification reactions as studied by scanning tunneling microscopy. *J. Am. Chem. Soc.* **1990**, *112*, 4598–4599.

[47] Hahn, J. R.; Kang, H.; Lee, S. M.; Lee, Y. H. Mechanistic study of defect-induced oxidation of graphite. *J. Phys. Chem. B* **1999**, *103*, 9944–9951.

[48] Mak, K. F.; He, K. L.; Lee, C.; Lee, G. H.; Hone, J.; Heinz, T. F.; Shan, J. Tightly bound trions in monolayer MoS_2. *Nat. Mater.* **2013**, *12*, 207–211.

[49] Chakraborty, B.; Bera, A.; Muthu, D. V. S.; Bhowmick, S.; Waghmare, U. V.; Sood, A. K. Symmetry-dependent phonon renormalization in monolayer MoS_2 transistor. *Phys. Rev. B* **2012**, *85*, 161403.

[50] Das, A.; Pisana, S.; Chakraborty, B.; Piscanec, S.; Saha, S. K.; Waghmare, U. V.; Novoselov, K. S.; Krishnamurthy, H. R.; Geim, A. K.; Ferrari, A. C. et al. Monitoring dopants by Raman scattering in an electrochemically top-gated graphene transistor. *Nat. Nanotechnol.* **2008**, *3*, 210–215.